Robust Image Registration using Adaptive Expectation Maximisation based PCA

Parminder Singh Reel†, Laurence S. Dooley†, K. C. P. Wong†, Anko Börner⋆

†*Department of Computing and Communications, The Open University, Milton Keynes, United Kingdom*
⋆*Optical Sensor Systems, German Aerospace Center (DLR), Berlin, Germany*

Email: †{parminder.reel, laurence.dooley, k.c.p.wong}@open.ac.uk, ⋆anko.boerner@dlr.de

***Abstract*—Images having either the same or different modalities can be aligned using the systematic process of image registration. Inherent image characteristics including intensity non-uniformities in magnetic resonance images and large homogeneous non-vascular regions in retinal and other generic image types however, pose a significant challenge to their registration. This paper presents an *adaptive expectation maximisation for principal component analysis with mutual information* (*a*EMPCA-MI) similarity measure for image registration. It introduces a novel iterative process to adaptively select the most significant principal components using Kaiser rule and applies 4-pixel connectivity for feature extraction together with Wichard's bin size selection in calculating the MI. Both quantitative and qualitative results on a diverse range of image datasets, conclusively demonstrate the superior image registration performance of *a*EMPCA-MI compared with existing MI-based similarity measures.**

***Index Terms*—Principal component analysis.**

I. Introduction

Registration of mono and multimodal images is a fundamental processing task for many computer vision and imaging based applications [1], such as in registering human brain and retinal images to assist in disease diagnosis and treatment planning. Brain and retinal *image registration* (IR) is particularly demanding due to the presence of inherent artefacts such as *intensity non-uniformities* (INU) in *magnetic resonance images* (MRI) [2] or the latent large homogeneous non-vascular regions [3] in retinal images. These collectively make the process of physically aligning a reference and sensed (source) image to maximise some predefined similarity measure (SM) [1] very challenging.

Various SM for IR have been proposed [1] which can be broadly categorized according to whether they are based on cross correlation, Fourier techniques and *mutual information* (MI) [4]. MI exploits the statistical relationship between the sensed and reference images and has been proven to be computationally efficient and well-established in the medical imaging domain [4]. It is however, very sensitive to interpolation artefacts in the presence of INU and can be seriously compromised when overlapping areas are small. In contrast, *regional* MI (RMI) [5] uses neighbourhood region features for MI by segmenting an image into several regions for feature extraction, so reducing the influence of INU upon IR quality. Its drawback however, is that it employs a covariance matrix for entropy approximation and as region expands, so commensurately does the computational complexity [5].

Recently, the *expectation maximisation for principal component analysis with MI* (EMPCA-MI) algorithm [6] has been shown to considerably lower the computational cost without loss of IR performance for dissimilar imaging modalities of the human anatomy [7]. It achieves dimensionality reduction by iteratively computing the first principal component instead of solving the complete covariance matrix as in conventional *principal component analysis* (PCA) [8]. It has subsequently been refined as *modified* EMPCA-MI (*m*EMPCA-MI) [9] which uses *8-pixel* and *4-pixel* connectivity for rearranging the neighbourhood data values to preserve both the spatial and intensity information, thus leading to superior IR performance. This gave the impetus to formalise the EMPCA-MI SM such that, it is able to adaptively determine the most appropriate number of principal components to represent prominent features in a particular dataset.

Various approaches to selecting the best subset of significant principal components have been proposed including Scree Graph, Broken-stick and their variants [8], which choose the subset by computing the cumulative variance of all components. In contrast, the Kaiser Rule [8] retains only those principal components whose eigenvalues are greater than one. It considers the variables in the image data to be independent and so their principal components are the same as variables, having unity variance in the case of the correlation matrix. This important attribute of the Kaiser Rule is image dependent [8], so it can automatically determine the number of significant principal components required to represent image features for a prescribed accuracy. Furthermore, it is well suited to EMPCA-MI since it iteratively determines the principal components in descending order of eigenvalues. These two distinct characteristics provided the motivation to incorporate the Kaiser Rule into the EMPCA-MI framework.

This paper presents an *adaptive* EMPCA-MI (*a*EMPCA-MI) SM which employs *4-pixel* connectivity neighbourhood region for pre-processing in combination with a Kaiser Rule based, EMPCA computation of significant principal com-

978-1-4799-6139-9/14/$31.00

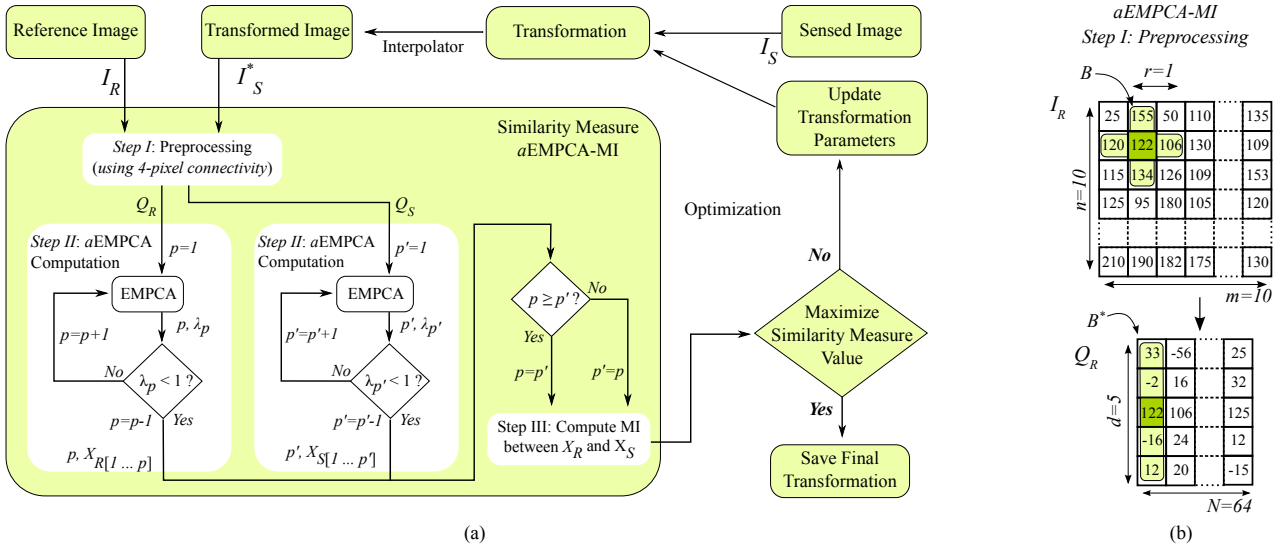

Fig. 1. (a) Registration Framework for the *a*EMPCA-MI algorithm. (b) Illustration of the pre-processing *Step I* with *4-pixel* region connectivity for an image pair size of *10* × *10* pixels.

ponents for both the reference and sensed images. These respective components are then used to calculate the MI. *a*EMPCA-MI enables better representation of image features compared to the conventional EMPCA-MI [6] which only used the first dominant principal component. Numerical and qualitative results confirm *a*EMPCA-MI provides lower IR errors in comparison with both EMPCA-MI and other SM for a variety of test image datasets.

The remainder of the paper is as follows: Section II describes the principles of IR and introduces the new *a*EMPCA-MI algorithm. Section III describes the experimental setup and test image datasets used together with a critical results analysis. Finally, Section IV provides some concluding comments.

II. Adaptive EMPCA-MI based Image Registration

A. IR Principles

IR is a multistage process which seeks to align a sensed image I_S with a reference image I_R [1] and generally involves the following key steps: *i)* transforming the coordinates of I_S with known transformation parameters in a given reference space; *ii)* generating a new interpolated source image $I_S^\star$ in the reference space; *iii)* comparing $I_S^\star$ with I_R using a SM; and *iv)* optimising the transformation parameters sequentially, to attain the best possible alignment, where the SM value is a maximum between the two images. The IR process for the proposed *a*EMPCA-MI is visualised in Fig.1(a) and is detailed in the following section.

B. aEMPCA-MI Similarity Measure

The new SM comprises three constituent steps (see Fig.1(a)). It first pre-processes the neighbourhood information for both I_S and I_R, before adaptively computing the principal components, and finally calculating the MI.

1) Step I — Pre-processing: This derives a second-order representation of the image grayscale values by using *4-pixel* connectivity neighbourbood as in [9]. This process helps to retain the local spatial neighbourhood relationship rather than pixel values as in [6], which leads to distinctive repetitive patterns. To illustrate this, consider the example of I_R in Fig.1(b), for a sliding window of radius r with *c-pixel* connectivity in neighbourhood B (with *r=1* and *c=4*). The resulting ith element, where $1 \leq i \leq c{+}1$ of single dimension vector B^* of length $c{+}1$, can be expressed as:

$$B_i^* = \begin{cases} B_i - B_{\frac{c}{2}+1} & if\ i \leq \frac{c}{2}+1\ and\ i > \frac{c}{2}+1 \\ B_i & if\ i = \frac{c}{2}+1 \end{cases} \quad (1)$$

Each column vector B^* now represents the differential value of c connected pixels with respect to the centre pixel $B_{\frac{c}{2}+1}$. These vectors are concatenated as Q_R with dimensions $d \times N$ where d represents the dimensional space i.e., $d{=}c{+}1$ in the example in Fig.1(b) and N is the number of pixels scanned (excluding the boundary pixels). Similar preprocessing step are performed on $I_S^\star$ to generate Q_S.

2) Step II — Compute aEMPCA: This dimensionality reduction step for Q_R and Q_S uses Kaiser Rule [8] to adaptively find the significant principal components using EMPCA [6]. The flowchart in Fig.1(a) shows how the *a*EMPCA algorithm adaptively computes and retains the first p principal components from Q_R having eigenvalue $\lambda_p > 1$ (similarly compute p' components for Q_S). These components are then concatenated as X_R and X_S respectively. The order of computational complexity for *a*EMPCA is $\mathcal{O}(Npr^2)$ which given that $N \gg p, r$ is the same as that incurred by EMPCA i.e. $\mathcal{O}(N)$, though due to the iterative nature of the algorithm its overall time overhead will tend to be slightly higher. Note that when *p=1*, EMPCA [6] becomes a special case of *a*EMPCA.

3) Step III — Compute MI: This final step determines the MI [4] between the highest number of common principal components in both X_R and X_S of the reference and sensed

TABLE I
DATASET PARAMETERS

Dataset	*Resolution (pixels)*	*INU*	*Noise(β)*
MRI T1 (T1)	[181 × 217 × 181]	α_{20}=20% INU	Gaussian (μ=0.01, and σ^2=0.01)
MRI T2 (T2)	[181 × 217 × 181]	α_{40}=40% INU	
Lena (*L*)	[256 × 256]	$Z(x,y)=\frac{1}{3.2}(x+y)$	
Baboon (*Bb*)	[256 × 256]		
Fundus (*F*)	[3888 × 2592]	-	-
SLO (*SLO*)	[768 × 768]		

images. The *Wichard* approach [10] has been used to select the best bin size in computing the individual and joint probabilities, since it exploits the *kurtosis* measure of the data distribution rather than applying the traditional fixed bin-size approach for accurate MI computation [11].

III. EXPERIMENTAL EVALUATION

A. Experimental Setup and Datasets

A series of IR experiments were undertaken to analyse the comparative performance of the *a*EMPCA-MI on a range of diverse image datasets. Multimodal MRI T1 and T2 datasets from the *BrainWeb* database [12] were chosen due to their challenging INU and noise artefacts with the corresponding parameter details being defined in Table I. To reflect the broad range of IR applications and evaluate the robustness of *a*EMPCA-MI, the well-known *Lena* (*L*) and *Baboon* (*Bb*) images were used in combination with an INU function [6], and additive Gaussian noise. In addition, a clinical monomodal retinal colour *Fundus* (*F*) IR was performed followed by multimodal *F* and *Scanning Laser Ophthalmoscope* (*SLO*) IR. These retinal images are inherently characterised by non-uniform illumination and large homogeneous non-vascular regions which render them especially challenging for IR, though neither INU nor noise was added to the retinal datasets because they are not prominent in the acquisition process [3]. Various IR experiments using the aforementioned datasets were conducted and classified into six *Scenarios* as shown in Table II. The transformation model consisted of (*X*, *Y*, θ, *S*), where *X* and *Y* are the respective translations along the *x* and *y* axis, θ is the rotational motion and *S* is a scaling factor.

In *Scenarios 1 — 4*, *S=1* so ΔS*=0*, while in *Scenarios 5* and *6*, since these involve retinal images, the magnification changes can result from using different equipment or the motion in the direction of the optical axis which can vary the value of *S*. To establish the requisite ground truth, all images were mis-registered by a known transformation, with the original images then being considered as I_S. The (*X*, *Y*, θ, *S*) settings where the *a*EMPCA-MI is a maximum are then considered the best image alignment.

To critically analyse the IR performance, the percentage *registration error* (RE) [1] between the initial and final value for each parameter was determined. In order to equitably reflect the computational time incurred for each SM, the corresponding *average run time* (ART) was calculated for every IR iteration. The RE performance of *a*EMPCA-MI was evaluated against four existing MI-based SM for six *Scenarios*, with the results displayed in Table II, where all parameter settings are kept constant for each SM, except the adaptive number of principal components in *a*EMPCA-MI. The IR process used partial volume interpolation along with Powell's optimization method [1]. All experiments were performed on Ubuntu 10.04 with 2.93 GHz Intel Core and 3GB RAM, and the assorted algorithms were all implemented in MATLAB.

B. Result Discussion

To clarify the nomenclature adopted in Table II; T1+α_{20} for example, represents a MRI T1 image slice with 20% INU, while *Bb*+*Z*+β is the *Baboon* image with INU and Gaussian noise artefacts. For *a*EMPCA-MI, the corresponding *p* value is displayed alongside the IR errors and signifies the number of adaptively determined principal components. Fig.2(a) displays the ART for three *Scenario* groups and while the ART is resource dependent, it is still an insightful time cost metric. The RE results confirm that the new *a*EMPCA-MI algorithm provides superior IR in all six *Scenarios*, including the challenging *Scenario 6*. For example, a significantly lower RE is observed for *a*EMPCA-MI in *Scenario 2* for T1+α_{40}+β with T2 with a percentage RE of (*8.72*, *2.95*, *0.51*, *0.00*) contrasting with both EMPCA-MI [6] (*9.70*, *4.30*, *0.62*, *0.00*)

TABLE II
REGISTRATION ERROR FOR SIX SCENARIOS, WHERE ΔS*=0* FOR SCENARIOS 1 - 4.

Scen. No.	I_R	I_S	MI [4]	RMI [5] (*r=1*)	EMPCA-MI [6] (*r=1*)	*m*EMPCA-MI [9] (*4-pixel*, *r=1*)	*a*EMPCA-MI (*r=1*)		
			ΔX, ΔY, $\Delta\theta$, ΔS	ΔX, ΔY, $\Delta\theta$, ΔS	ΔX, ΔY, $\Delta\theta$, ΔS	ΔX, ΔY, $\Delta\theta$, ΔS	*p*	ΔX, ΔY, $\Delta\theta$, ΔS
1	T1+α_{20}	T1	9, 6.0, 0.5, 0.00	5.20, 4.00, 0.44, 0.00	2.00, 1.30, 0.36, 0.00	1.12, 0.93, 0.21, 0.00	2	1.02, 0.90, 0.18, 0.00
	T1+α_{40}		10, 8.3, 0.7, 0.00	6.20, 5.30, 0.50, 0.00	4.50, 4.00, 0.42, 0.00	2.96, 3.04, 0.32, 0.00	3	2.25, 2.89, 0.27, 0.00
	T1+$\alpha_{40}+\beta$		13, 16, 0.9, 0.00	10.5, 13.3, 0.60, 0.00	8.00, 10.0, 0.58, 0.00	7.45, 9.28, 0.46, 0.00	3	7.19, 9.21, 0.42, 0.00
2	T1+α_{20}	T2	11, 8.3, 0.5, 0.00	7.00, 7.00, 0.48, 0.00	2.60, 2.60, 0.42, 0.00	1.93, 1.71, 0.32, 0.00	2	1.80, 1.51, 0.29, 0.00
	T1+α_{40}		12, 9.6, 0.7, 0.00	8.00, 9.00, 0.57, 0.00	4.80, 4.60, 0.62, 0.00	3.98, 4.10, 0.43, 0.00	2	3.62, 3.92, 0.41, 0.00
	T1+$\alpha_{40}+\beta$		14, 19, 1.8, 0.00	14.0, 19.3, 0.58, 0.00	9.70, 4.30, 0.62, 0.00	8.99, 3.11, 0.56, 0.00	4	8.72, 2.95, 0.51, 0.00
3	$L+Z$	*L*	0.4, 0.5, 0.2, 0.00	0.20, 0.38, 0.21, 0.00	0.20, 0.32, 0.21, 0.00	0.16, 0.24, 0.17, 0.00	3	0.15, 0.23, 0.13, 0.00
	$L+Z+\beta$		14, 19, 0.4, 0.00	9.00, 13.6, 0.24, 0.00	2.00, 5.33, 0.21, 0.00	1.93, 5.26, 0.19 , 0.00	4	1.91, 5.23, 0.18, 0.00
4	$Bb+Z$	*Bb*	12, 3.5, 0.2, 0.00	0.60, 1.06, 0.21, 0.00	0.45, 0.70, 0.21, 0.00	0.30, 0.60, 0.16, 0.00	3	0.28, 0.59, 0.14, 0.00
	$Bb+Z+\beta$		13, 17, 0.3, 0.00	2.00, 2.60, 0.20, 0.00	1.40, 1.50, 0.23, 0.00	1.20, 1.22, 0.20, 0.00	4	1.15, 1.22, 0.19, 0.00
5	*F*	*F*	1.2, 1.8, 0.6, 0.2	0.12, 0.16, 0.32, 0.21	0.11, 0.13, 0.17, 0.14	0.10, 0.12, 0.16, 0.13	2	0.10, 0.10, 0.13, 0.10
6	*F*	*SLO*	2.1, 1.9, 0.8, 0.5	0.32, 0.41, 0.49, 0.42	0.29, 0.37, 0.41, 0.39	0.25, 0.34, 0.38, 0.37	2	0.22, 0.31, 0.36, 0.34

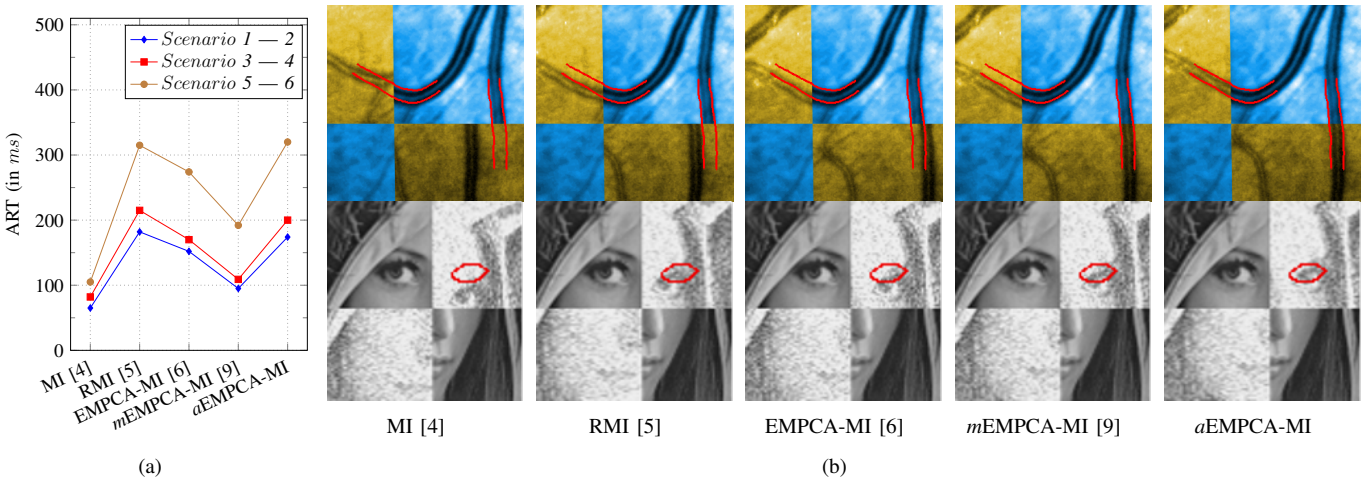

Fig. 2. (a) ART performance for various SM (b) Checkerboard Overlay [1] IR results (zoomed-in); top: F with *SLO* (*Scenario 6*) and bottom: $L + Z + \beta$ with L (*Scenario 3*) with ground truth in *red*.

and *m*EMPCA-MI [9] (*8.99*, *3.11*, *0.56*, *0.00*). This is due to *a*EMPCA-MI using *4-pixel* neighbourhood and *p=4*.

Conversely, both EMPCA-MI and *m*EMPCA-MI use just a single principal component, which can in certain circumstances limit the IR accuracy. This performance improvement for *a*EMPCA-MI however, is counterbalanced by a slower ART of *174ms* due to its iterative nature as compared with *152ms* and *95ms* for EMPCA-MI and *m*EMPCA-MI respectively. Similar RE trends are evident in the *Lena*, *Baboon* and retinal datasets with *a*EMPCA-MI again consistently outperforming the comparators, due to more principal components being used in the MI computation, which ultimately leads to enhanced IR.

Particularly noteworthy is the IR performance of *a*EMPCA-MI in the challenging *Scenarios 5* and *6* where *p=2* is adaptively chosen due to the large homogeneous non-vascular regions in the *Fundus* and *SLO* images, providing the lowest RE in both *Scenarios*. Despite reducing the data dimensionality by using *4-pixel* connectivity the performance offset for this improved IR is the higher ART of *320ms* because of the high resolution of the *Fundus* images. A similar observation on the computational cost is apparent in other *Scenarios*, as an inevitable outcome of the adaptive process inherent in the new *a*EMPCA-MI.

Fig.2(b) displays qualitative IR results using the checkerboard overlaying [1] technique for *Fundus* and *Lena* images. The perceptual IR results for the F with *SLO* IR in *Scenario 6* can be evaluated by checking the continuity of vessel structures (colour enhanced for higher visibility) and similarly with the positioning of the eyes for IR between $L+Z+\beta$ with L in *Scenario 3* (with the ground truth in *red*) . These results palpably validate that the new *a*EMPCA-MI consistently provides superior IR and lower RE, while recognizing the computational cost trade-off required to achieve the improved IR robustness to INU, noise and large homogeneous features.

IV. Conclusion

This paper has presented an adaptive dimension to the existing *Expectation Maximisation for Principal Component Analysis with MI* (EMPCA-MI) similarity measure. Enhanced IR performance for clinical and generic images exhibiting a range of challenging features including INU, Gaussian noise and large homogeneous regions confirms the efficacy of the *a*EMPCA-MI algorithm. This is achieved by adaptively incorporating more significant principal components with a corresponding trade-off in terms of computational overheads.

References

[1] B. Zitová and J. Flusser, "Image registration methods: a survey," *Image Vision Comput.*, vol. 21, no. 11, pp. 977–1000, Oct. 2003.
[2] A. Simmons, P. S. Tofts, G. J. Barker, and S. R. Arridge, "Sources of intensity nonuniformity in spin echo images at 1.5 t," *Magn. Reson. Med.*, vol. 32, no. 1, pp. 121–128, Jul. 1994.
[3] P. J. Saine and M. E. Tyler, *Ophthalmic photography : retinal photography, angiography, and electronic imaging*. Boston: Butterworth-Heinemann, 2002.
[4] P. Viola and W. M. Wells III, "Alignment by maximization of mutual information," *Int J Comput Vision*, vol. 24, no. 2, pp. 137–154, 1997.
[5] D. B. Russakoff, C. Tomasi, T. Rohlfing, and C. R. Maurer, "Image similarity using mutual information of regions," in *ECCV '04*. Springer, 2004, vol. 3023, pp. 596–607.
[6] P. S. Reel, L. S. Dooley, and K. C. P. Wong, "Efficient image registration using fast principal component analysis," in *ICIP*, 2012, pp. 1661–1664.
[7] P. S. Reel, L. S. Dooley, K. C. P. Wong, and A. Börner, "Robust retinal image registration using expectation maximisation with mutual information," in *ICASSP*, 2013, pp. 1118–1122.
[8] I. T. Jolliffe, *Principal component analysis*, 2nd ed., ser. Springer series in statistics. New York: Springer, 2002, 00248.
[9] P. S. Reel, L. S. Dooley, K. C. P. Wong, and A. Börner, "Fast EM principal component analysis image registration using neighbourhood pixel connectivity," in *CAIP*. Springer, 2013, vol. 8047, pp. 270–277.
[10] J. Wichard, R. Kuhne, and A. T. Laak, "Binding site detection via mutual information," in *IEEE FUZZ '08*, 2008, pp. 1770–1776.
[11] P. S. Reel, L. S. Dooley, K. C. P. Wong, and A. Börner, "Enhanced retinal image registration accuracy using expectation maximisation and variable bin-sized mutual information," in *ICASSP*, 2014, pp. 6682–6686.
[12] C. A. Cocosco, V. Kollokian, R. K.-S. Kwan, G. B. Pike, and A. C. Evans, "Brainweb: Online interface to a 3d mri simulated brain database," *NeuroImage*, vol. 5, p. 425, 1997.